AIP | Journal of Applied Physics

Thermoelectric properties of Zn5Sb4In2-δ (δ=0.15)

Y. Wu, A. P. Litvinchuk, E. S. Toberer, G. J. Snyder, N. Newman et al.

Citation: J. Appl. Phys. **111**, 123712 (2012); doi: 10.1063/1.4729566
View online: http://dx.doi.org/10.1063/1.4729566
View Table of Contents: http://jap.aip.org/resource/1/JAPIAU/v111/i12
Published by the American Institute of Physics.

Related Articles

A Thomson scattering diagnostic on the Pegasus Toroidal experiment
Rev. Sci. Instrum. 83, 10E335 (2012)

Fully automated measurement setup for non-destructive characterization of thermoelectric materials near room temperature
Rev. Sci. Instrum. 83, 074904 (2012)

Polychromator for the edge Thomson scattering system in ITER
Rev. Sci. Instrum. 83, 10E328 (2012)

Power factor enhancement in light valence band p-type skutterudites
Appl. Phys. Lett. 101, 022101 (2012)

Increased electrical conductivity in fine-grained (Zr,Hf)NiSn based thermoelectric materials with nanoscale precipitates
Appl. Phys. Lett. 100, 254104 (2012)

Additional information on J. Appl. Phys.

Journal Homepage: http://jap.aip.org/
Journal Information: http://jap.aip.org/about/about_the_journal
Top downloads: http://jap.aip.org/features/most_downloaded
Information for Authors: http://jap.aip.org/authors

ADVERTISEMENT

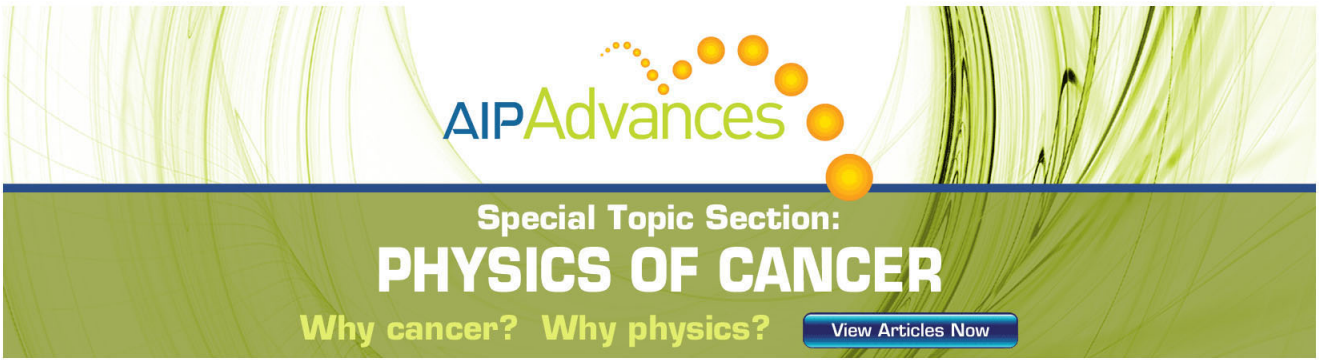

Downloaded 30 Jul 2012 to 131.215.220.186. Redistribution subject to AIP license or copyright; see http://jap.aip.org/about/rights_and_permissions

Thermoelectric properties of $Zn_5Sb_4In_{2-\delta}$ ($\delta = 0.15$)

Y. Wu,[1,a)] A. P. Litvinchuk,[2] E. S. Toberer,[3] G. J. Snyder,[4] N. Newman,[5] A. Fischer,[6] E.-W. Scheidt,[6] W. Scherer,[6] and U. Häussermann[1,b)]
[1]*Department of Chemistry and Biochemistry, Arizona State University, Tempe, Arizona 85287-1604, USA*
[2]*TCSUH and Department of Physics, University of Houston, Houston, Texas 77204-5002, USA*
[3]*Physics Department, Colorado School of Mines, Golden, Colorado 80401, USA*
[4]*Materials Science, California Institute of Technology, 1200 East California Boulevard, Pasadena, California 91125, USA*
[5]*School of Materials, Arizona State University, Tempe, Arizona 85287-8706, USA*
[6]*Department of Physics, Augsburg University, D-86159 Augsburg, Germany*

(Received 24 April 2012; accepted 17 May 2012; published online 21 June 2012)

The polymorphic intermetallic compound $Zn_5Sb_4In_{2-\delta}$ ($\delta = 0.15(3)$) shows promising thermoelectric properties at low temperatures, approaching a figure of merit *ZT* of 0.3 at 300 K. However, thermopower and electrical resistivity changes discontinuously at around 220 K. Measurement of the specific heat locates the previously unknown temperature of the order-disorder phase transition at around 180 K. Investigation of the charge carrier concentration and mobility by Hall measurements and infrared reflection spectroscopy indicate a mixed conduction behavior and the activation of charge carriers at temperatures above 220 K. $Zn_5Sb_4In_{2-\delta}$ has a low thermal stability, and at temperatures above 470 K samples decompose into a mixture of Zn, InSb, and Zn_4Sb_3. © *2012 American Institute of Physics*. [http://dx.doi.org/10.1063/1.4729566]

I. INTRODUCTION

Binary compounds between zinc and antimony have attracted a lot of attention due to their thermoelectric properties.[1–4] In particular p-type, β-Zn_4Sb_3 is considered as a state-of-the-art material for the temperature region 400–700 K and thus interesting for waste heat recovery applications from automotive exhausts.[5,6] However, a notorious problem of Zn_4Sb_3 manifests in its limited thermal stability which has hampered the development of practical devices.[7] Computational modeling studies confirm that β-Zn_4Sb_3 is only weakly stable with respect to decomposition into Zn and ZnSb.[8]

Ternary derivatives of zinc antimonides may show improved thermal stability while still providing good thermoelectric properties. Accordingly, the recently discovered compound $Zn_5Sb_4In_{2-\delta}$ ($\delta = 0.15$) outperforms Zn_4Sb_3 in the low temperature range 10 – 350 K.[9] It crystallizes in a novel orthorhombic framework structure (shown in Fig. 1) that can be looked upon as a stuffed variant of the prolific tetragonal $CuAl_2$ type ($1 \times 2 \times 1$ superstructure). The arrangement of Sb atoms is identical to that of the Al atoms in $CuAl_2$ and corresponds to rows of face-sharing square antiprisms that are connected in the *bc* plane by sharing triangle edges. The majority of Zn atoms occupies tetrahedral interstices in the Sb substructure and attains a peculiar five-coordination by one like and four Sb atoms, which is typical for the structures of binary zinc antimonides. The remaining Zn and In atoms are distributed in the tetragonal channels formed by the square antiprisms and display some disorder. For Zn, this is expressed in a split position and for In in an occupational deficiency (5%–10%), which is indicated as δ in the compound formula. At temperatures below 200 K, $Zn_5Sb_4In_{2-\delta}$ undergoes a phase transition into a more ordered structure where the Zn split position resolves in a monoclinic space group without a change of the unit cell.[9]

From theoretical calculations, it has been shown that when considering an ideal situation with fully occupied In positions ($\delta = 0$), monoclinic $Zn_5Sb_4In_{2-\delta}$ possesses a narrow band gap with a size of 0.2 eV, and the Fermi level becomes situated at this gap.[10] The In deficiency may shift the Fermi level into the valence band, and thus determine the p-type carrier concentration. This situation would be similar to β-Zn_4Sb_3, where the p-type carrier concentration is controlled by a small width of Zn deficiency.[11] The electrical resistivity ρ and thermopower (or Seebeck coefficient) *S* of $Zn_5Sb_4In_{2-\delta}$ are typical of a heavily doped or degenerate semiconductor. Both properties, however, change discontinuously at around 220 K.[9] The altered behavior of *S* is detrimental to the thermoelectric figure of merit ZT ($Z = S^2/\rho\kappa$) at higher temperatures, where κ is the thermal conductivity. The nature of the temperature dependency of ρ and *S* for $Zn_5Sb_4In_{2-\delta}$ is not yet understood. In this work, we elucidate whether there is a relation between the discontinuous property changes of $Zn_5Sb_4In_{2-\delta}$ and the monoclinic-to-orthorhombic structural transition, and study the charge carrier concentration and dynamics across a temperature range covering both events. Furthermore, investigations into the thermal stability of $Zn_5Sb_4In_{2-\delta}$ are performed.

II. EXPERIMENTAL SECTION

A. Synthesis and phase characterization

$Zn_5Sb_4In_{2-\delta}$ was synthesized by the flux procedure described in detail in Refs. 9 and 12. This method affords $Zn_5Sb_4In_{2-\delta}$ as phase-pure, mm-sized, typically agglomerated,

a)Present address: Department of Physics, Tsinghua University, Bejing, China, 100084.
b)E-mail: Ulrich.Haussermann@asu.edu.

 © 2012 American Institute of Physics

Downloaded 30 Jul 2012 to 131.215.220.186. Redistribution subject to AIP license or copyright; see http://jap.aip.org/about/rights_and_permissions

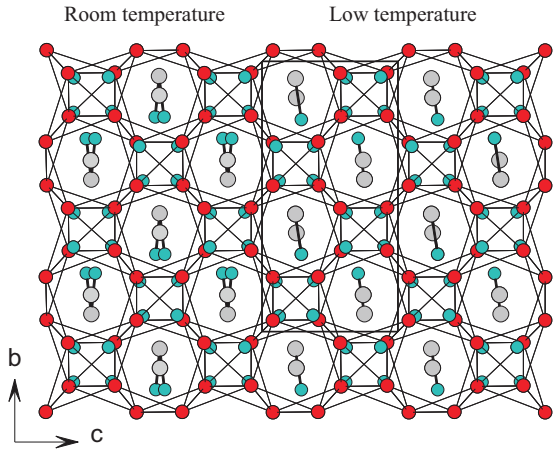

FIG. 1. The structure of the orthorhombic room temperature and monoclinic low temperature form of $Zn_5Sb_4In_{2-\delta}$ projected along the *a* direction. Cyan, red, and grey circles denote Zn, Sb, and In atoms, respectively. The Sb substructure corresponding to rows of face-sharing square antiprisms is shown by thin lines. Atom pairs Zn-Zn and Zn-In stuffing tetragonal channels are connected by thick lines.

crystals. Such crystal pieces were selected and processed for the various investigations:

Specimen A1 and A2: Large (non-agglomerated) crystal specimens were carefully shaped and polished into square blocks with dimensions $4.50 \times 4.50 \times 0.62$ mm and $3.84 \times 3.84 \times 0.40$ mm, respectively. The surface of the obtained specimen was free from any excess metal residual from the flux synthesis.

Specimen B (cold pressed sample): crystal specimens obtained from flux synthesis were ground to a fine powder and pressurized to 2 GPa at room temperature in a multi anvil device.[13] The obtained specimen corresponded to a cylinder (4.2 mm in diameter and 8.0 mm in length) with a density close to the crystallographic density of $Zn_5Sb_4In_{2-\delta}$ (>98%). From this cylinder, disks with 0.5 mm thickness were cut with a diamond saw.

For phase analysis of samples obtained from flux synthesis and of specimens obtained after further processing, powder x-ray diffraction (PXRD) patterns were collected on a Siemens D5000 diffractometer (Bragg-Brentano θ:θ geometry) using Cu Kα radiation ($\lambda = 1.54059$ Å). Scanning electron microscopy (SEM) was employed to examine the surfaces of samples by back scattered electron imaging and energy dispersive spectroscopy (EDS). The SEM studies were performed in an FEI XL-30 scanning electron microscope.

B. Thermal analysis

Differential scanning calorimetry (DSC) measurements were carried out on a TA Instrument 2910 calorimeter. Weighed samples of ~20 mg were sealed in TA Tzero aluminum pans under dry argon. All experiments were performed with a helium flow of ~30 ml/min. Baselines were collected with two empty pans to determine the heat imbalance between the sample and reference pan. Temperature and heat flow were calibrated with indium ($T_m = 429.8$ K, $\Delta H = 28.58$ J/g) and zinc ($T_m = 692.7$ K). Scanning temperatures ranged from room temperature to 723 K at a heating and cooling rate of 5 K/min. Data processing and analysis were made with the TA Instrument software Universal Analysis 2000.

C. Heat capacity measurement

The temperature-dependent heat capacity was measured from 300 K to 2 K (50 points distributed logarithmically) using a quasi-adiabatic step heating technique as implemented in the physical property measurement system (PPMS) of Quantum Design. A sample prepared by grinding crystal specimens of $Zn_5Sb_4In_{2-\delta}$ (approx. 10 mg) was thermally connected to the platform of the sample-holder via small amount of Apiezon-N grease. In addition, the measurement was repeated from 210 K to 130 K (50 points distributed linearly) in order to get a detailed description of the phase transition, and from 300 K to 270 K (four points distributed linearly) to get a better support for the theoretical match in this region. The uncertainty of the measurement is estimated to be below 5%.

D. Transport measurements

Hall and resistivity measurements were carried out on specimens A1, A2, and B in a custom computer-controlled system designed in the van der Pauw configuration. The Hall coefficient is defined as

$$R_H = \frac{V_H d}{IB} = -\frac{1}{n_H q}, \tag{1}$$

where V_H is the Hall voltage, I is the current through the sample, B is the magnetic flux density, and d is the thickness of the sample. Further, n_H is the Hall carrier concentration and q is the carrier charge ($-$e or $+$e for electrons and holes, respectively). The resistivity from the van der Pauw configuration was calculated according to Ref. 14. The entire system consisted of a $7\frac{1}{2}$ Agilent 34420 A voltmeter, a high impendence Keithley 7065 Hall card in a Keithley 7001 switch matrix, and a Keithley 200 current source. Four contacts with gold wires were painted with Demetron D200 silver paint on the sample corners. The influence of the Nernst, Righi-Leduc, thermoelectric and geometric effects was eliminated by performing four sequential measurements in which the sign of the current and magnetic fields were reversed for opposing electrodes, followed by a similar sequence where the current and voltage electrode leads were switched. A set duration time of one second was used between the switching. The cryostat of the PPMS was employed to control the temperature from 10 to 350 K and to apply magnetic fields of 0.4 T perpendicular to the sample for the Hall measurements. The current used for both Hall and resistivity measurements was typically 10 mA. During the investigation of sample A2, a part of the specimen broke off. The Hall results for this sample were deemed unreliable and thus excluded.

Near normal incidence reflection spectra were recorded for specimen A2 with a Bomem DA-8 Fourier transform interferometer in the spectral range of 80–5000 cm^{-1} using a gold mirror as reference. Samples were mounted on the cold finger of a helium flow cryostat for temperature control.

Thermopower measurements were performed on samples A1 and B employing the thermal transport option (TTO)

Downloaded 30 Jul 2012 to 131.215.220.186. Redistribution subject to AIP license or copyright; see http://jap.aip.org/about/rights_and_permissions

of the PPMS. Two copper disks with extruded leads on each end were glued oppositely onto the specimen using a two-component silver-filled epoxy (Epo-Tek H20E), which provided contacts after curing at slightly elevated temperatures for a short time. The arrangement was then mounted on the TTO puck, which was subsequently loaded into the PPMS chamber and then evacuated ($<10^{-3}$ Torr) for the measurement. The measurements were conducted in a two-point configuration from 10 K to 350 K at a scanning rate of 0.3 K/min. For each specified measurement temperature, a heat pulse was applied to the sample to create a temperature gradient of 3%. The autorange feature of the PPMS system was used in all of the measurements. Radiation heat loss was automatically corrected with the incorporated functions of the software.

III. RESULTS AND DISCUSSION

A. Resitivity and thermopower

The peculiar feature of $Zn_5Sb_4In_{2-\delta}$ is a discontinuous change in the resistivity and thermopower at around 220 K. In Fig. 2(a), the resistivity for specimens A1, A2, and B is compared to the previously published resistivity of a crystalline sample.[9] In the interval 10–220 K, all samples show a metallic-like behavior until ρ reaches a maximum. Thereafter, ρ either plateaus (A1) or changes into a semiconductor-like behavior. The activation energy estimated from the exponential decrease of ρ for those samples is around 0.1 eV. Resistivity values for A2 appear higher than for the other samples. This, together with small changes in the slope at around 100 and 150 K, indicates a more complicated temperature dependence for this sample. The reason behind this behavior is unknown; however, we suspect that this sample actually was polycrystalline and of lower density than A1 and B.

The thermopower for $Zn_5Sb_4In_{2-\delta}$ samples exhibits a positive sign which implies that holes are the major charge carriers (Fig. 2(b)). Between 10 and 200 K, the temperature dependence of S is positive and S attains a maximum value at around 220 K. A discontinuity in the temperature dependence of S appears concomitant with that of the resistivity. The cold pressed sample (B) displays somewhat higher values of S. For an intrinsic semiconductor, the effective band gap E_g can be estimated according to $E_g = 2eT_{max}S_{max}$, where S_{max} is the maximum value of the thermopower and T_{max} is the temperature corresponding to the maximum of S.[15] Values for S_{max} and T_{max} around 200 μV/K and 200 K, respectively, result in E_g values around 0.08 eV, which agrees very well with the carrier activation energy obtained from the resistivity data.

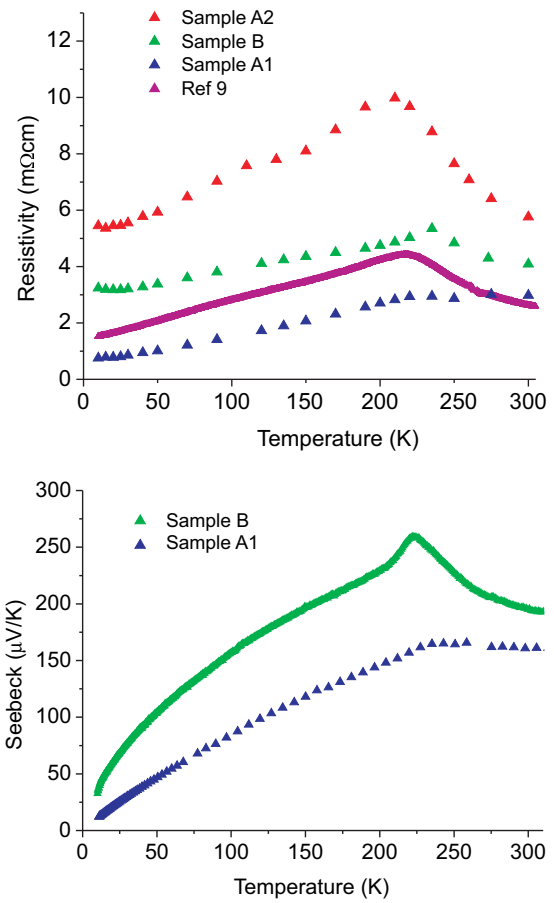

FIG. 2. Resistivity and thermopower (Seebeck coefficient) for different samples $Zn_5Sb_4In_{2-\delta}$ (A, crystalline; B, cold pressed).

B. Heat capacity

It may be suspected that the discontinuous property changes around 220 K are connected to the monoclinic-to-orthorhombic phase transition of $Zn_5Sb_4In_{2-\delta}$. This transformation is reversible and has been observed in single crystal x-ray diffraction experiments.[9] However, its temperature is not accurately known. The heat capacity measurement, shown in Fig. 3, displays an anomaly between approximately 125 and 200 K which peaks at around 180 K. To estimate the phonon contribution of the specific heat, a simple model with two Einstein modes ($T_{E1} = 175$ K and $T_{E2} = 361$ K) and one Debye contribution ($\Theta_D = 84$ K) was used and provided a good fit to the heat capacity for the data points above and below this anomaly. The individual contributions D:E1:E2 of the model

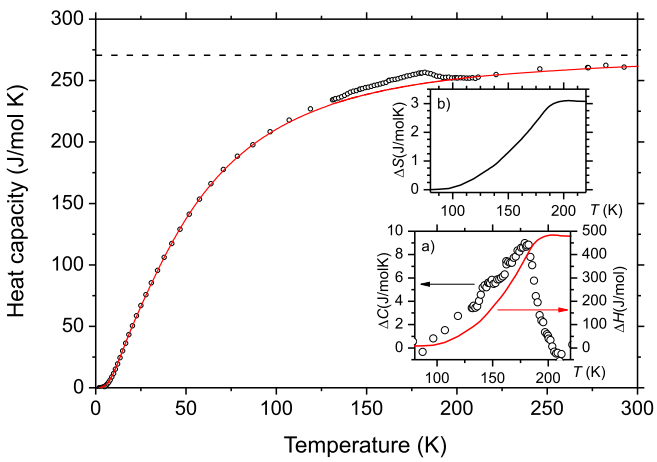

FIG. 3. Specific heat C (open circles) as a function of temperature T of $Zn_5Sb_4In_{2-\delta}$ together with the fitted phonon contribution (solid line) using a simple Debye-Einstein Model. The dashed line indicates the upper Dulong-Petit limit assuming $\delta = 0.15$. Inset (a) shows the broad anomaly ΔC (open circles) by subtraction of the phonon contribution from experimental data. The solid line represents the integrated enthalpy of the phase transition. Inset (b) displays the change in entropy of the phase transition.

Downloaded 30 Jul 2012 to 131.215.220.186. Redistribution subject to AIP license or copyright; see http://jap.aip.org/about/rights_and_permissions

were 4:5:1.85. We attribute the anomaly to the structural transformation and note that this transition occurs at lower temperatures with respect to the anomalies for S and ρ. Therefore, the two events are most likely not related. The enthalpy and entropy of the phase transition are 480 J/mol and 3.1 J/mol K, respectively. A rather high error of about 10% should be assigned to both values because of the uncertainly of the low temperature onset of the phase transition. The entropy value is slightly higher than for the order-disorder α-β transition in Zn_4Sb_3 (around 2 J/mol K).[16]

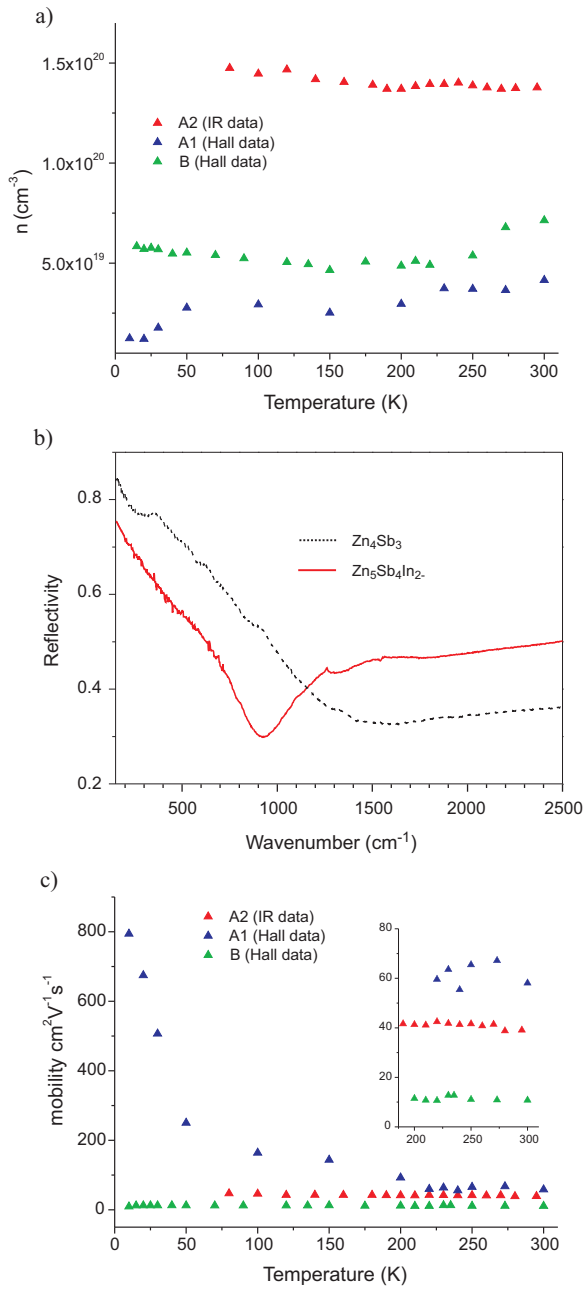

FIG. 4. (a) Carrier concentration for different samples $Zn_5Sb_4In_{2-\delta}$ (A, crystalline; B, cold pressed). (b) Reflectivity spectra for $Zn_5Sb_4In_{2-\delta}$ (red line, sample A2) and Zn_4Sb_3 (black, broken line) at 250 K. The spectrum for Zn_4Sb_3 is according to Ref. 18. (c) Mobility for different samples $Zn_5Sb_4In_{2-\delta}$ (A, crystalline; B, cold pressed).

C. Carrier concentration and mobility

Fig. 4(a) shows the carrier concentrations obtained from Hall measurements (A1 and B) and infrared reflectance spectroscopy (A2). The Hall carrier concentration ($n_H = 1/R_H e$) of the cold pressed sample B is around 6×10^{19} cm^3 at 10 K and appears to decrease slightly and linearly until 225 K after which a discontinuous change (increase) occurs. n_H for the crystalline sample A1 is just 1×10^{19} cm^3 at 10 K and increases to about 3×10^{19} cm^3 at around 50 K. At room temperature n_H is about 7 and 4×10^{19} cm^3 for B and A1, respectively. For β-Zn_4Sb_3 charge carrier concentrations at room temperature are in a range between 6 and 9×10^{19} cm^3; the interval is attributed to the slightly variable Zn content (self-doping).[11] Self-doping may also apply to $Zn_5Sb_4In_{2-\delta}$ considering slight variations in the In content. We note that n_H for A1 and B are reverse to what would have been expected from the resistivity and thermopower measurements (cf. Fig. 2).

Infrared reflection spectroscopy provides a means of contact-free measurement of carrier concentration and mobility. According to the Drude model, the oscillation of free charges with respect to the ions in the lattice can be considered as plasma, with a characteristic frequency ω_p

$$\omega_p^2 = \frac{4\pi n e^2}{\varepsilon_\infty m^*}, \tag{2}$$

where n is the charge carrier concentration, m^* is the effective mass, and ε_∞ is the complex dielectric constant at infinite frequency.[17] The dielectric constant function $\varepsilon(\omega)$ is obtained by a Kramer-Kronig transformation of reflection spectra. The imaginary part $\mathrm{Im}(-1/\varepsilon(\omega))$, also called electron energy loss function, provides information about ω_p (and thus the carrier concentration) from its peak position. The scattering rate of carriers, which is inversely proportional to the mobility, relates to the width of $\mathrm{Im}(-1/\varepsilon(\omega))$. Fig. 4(a) includes the carrier concentrations derived from optical reflectance spectra in the temperature range from 77 K to 300 K. For calculating carrier concentrations, an effective mass of 0.9 m_e was assumed. This value was found appropriate for Zn_4Sb_3.[16] We note that with this value for the effective mass, carrier concentrations obtained from spectroscopy are by about three times larger compared to the results from the Hall measurements. Since the value of m^* is uncertain it may be modified (diminished) to achieve a fit with the Hall carrier concentration. However, analysis of reflectance spectra shows that this simplification is not justified.

Reflectance spectra were collected for sample A2 between 100 and 300 K and did not show any significant temperature dependence. The spectrum at 250 K is shown representatively in Fig. 4(b), together with a corresponding spectrum for Zn_4Sb_3.[18] They are qualitatively similar in a sense that the reflectivity drops as frequency increases, reaches a minimum, and starts to increase again. The minimum, which is directly related to the "plasma edge," is situated at lower frequencies for $Zn_5Sb_4In_{2-\delta}$ in comparison with Zn_4Sb_3 (about 900 and 1500 cm^{-1}, respectively). This observation signals a considerable decrease of the ratio n/m^* for $Zn_5Sb_4In_{2-\delta}$. According to Eq. (2), when assuming similar

Downloaded 30 Jul 2012 to 131.215.220.186. Redistribution subject to AIP license or copyright; see http://jap.aip.org/about/rights_and_permissions

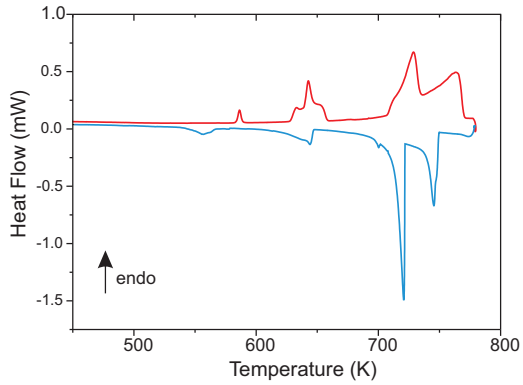

FIG. 5. DSC heating (red line) and cooling trace (blue line) of $Zn_5Sb_4In_{2-\delta}$.

carrier concentrations this suggests that m^* in $Zn_5Sb_4In_{2-\delta}$ is actually higher than in Zn_4Sb_3. Unfortunately, we were not able to perform Hall and reflectance measurements on the same specimen, which would have allowed to make a more conclusive assessment of the effective mass.

The charge carrier mobility was calculated from the Hall and optical reflectance spectroscopy data. This is shown in Fig. 4(c). The mobility extracted from the spectroscopically obtained scattering rate (sample A2) compares well with the Hall mobility of sample A1 in the temperature range 220–300 K. At room temperature, the values are 40 and 68 $cm^2V^{-1}s^{-1}$ for A2 and A1, respectively. These values are comparable with Zn_4Sb_3 but higher than for other complex intermetallic compounds considered for thermoelectric applications, such as $Yb_{14}Mn_{1-x}Al_xSb_{11}$ and $Ca_5Al_2Sb_6$.[19–21] The cold-pressed sample (B) displays a lower mobility (10 $cm^2V^{-1}s^{-1}$ at 300 K). Importantly, the mobility—being obtained from two independent experimental methods—does not show any significant discontinuity in the temperature dependence above 200 K and, thus, cannot be responsibly for the discontinuous resistivity change of $Zn_5Sb_4In_{2-\delta}$. For sample A1, the Hall mobility increases sharply when approaching low temperatures. This is a consequence of the sharp decrease of the carrier concentration. We note that sample A1 appeared highly crystalline, without noticeable cracks and defects. The behavior of sample A1 at low temperatures may be explained by a low concentration of extrinsic charge carriers and weak impurity scattering, due to a high degree of crystallinity.

It is important to recognize that neither spectroscopy nor Hall measurements indicate a substantial increase of the charge carrier concentration for $Zn_5Sb_4In_{2-\delta}$ at around 220 K, as perhaps expected from the altered temperature dependence of the resistivity. $Zn_5Sb_4In_{2-\delta}$ appears as a p-type material, however, considering the very small band gap (< 0.1 eV) conductivity may be actually of mixed type with substantial n-type contribution. In this case, Hall carrier concentrations shown in Fig. 4(a) would be too low because the equality in Eq. (1) is only valid for extrinsic conductors. This could explain why sample B displays a higher thermopower than sample A1 although its Hall carrier concentration according to Eq. (1) is higher. Also, the apparent issue with the effective mass may be explained by a mixed conduction scenario. The event at around 220 K could then correspond to a charge carrier activation, again of mixed type and with variable ratio. For example, for sample B, primarily majority carriers are excited, whereas the ratio is rather balanced for sample A1. This observation would agree with the previously made assumption that sample A1 is essentially intrinsic and displaying the highest degree of mixed type conduction. For sample A2, primarily minority carriers would be excited. Those remain undetected in IR reflection spectroscopy which probes the component with higher plasma frequency, i.e., the majority charge carrier. At this point, we are not able to prove

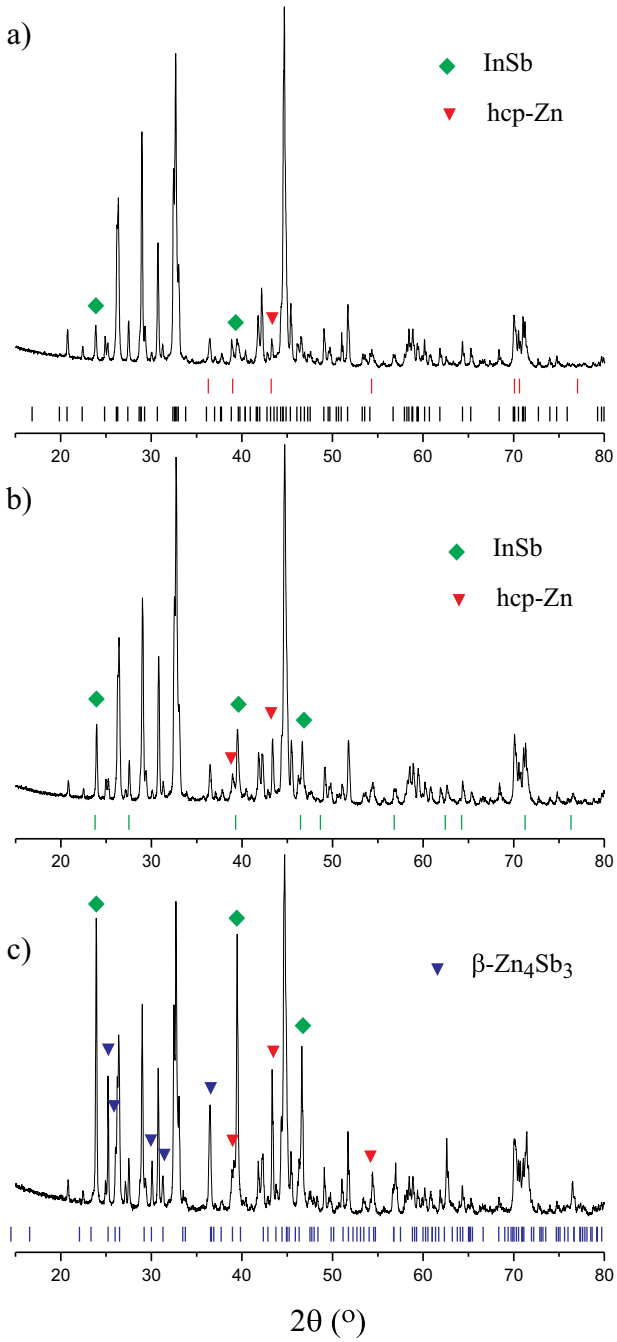

FIG. 6. Powder XRD pattern (Cu Kα) for annealed samples $Zn_5Sb_4In_{2-\delta}$ at 673 K (a), 723 K (b), and 773 K (c). Bragg positions for $Zn_5Sb_4In_{2-\delta}$ hcp-Zn, InSb and β-Zn_4Sb_3 are shown as black, red, green, and blue bars, respectively. Additionally, diamond and triangle symbols mark main reflections from the decomposition products.

Downloaded 30 Jul 2012 to 131.215.220.186. Redistribution subject to AIP license or copyright; see http://jap.aip.org/about/rights_and_permissions

explicitly a mixed conduction behavior but only hypothesize that it would provide a plausible explanation for the peculiar transport properties of $Zn_5Sb_4In_{2-\delta}$.

D. Thermal stability

The application of Zn_4Sb_3 in thermoelectric devices has been hampered by its low thermal stability and an interesting question is whether ternary derivatives provide an opening for this dilemma. Fig. 5 shows a DSC heating and cooling trace of $Zn_5Sb_4In_{2-\delta}$ from 450 to 750 K where multiple endothermic events can be identified. The endothermic peak around 590 K is most likely associated with a structural transition and perhaps even the events at around 690 K. At higher temperatures, the decomposition of $Zn_5Sb_4In_{2-\delta}$ into a mixture of Zn_4Sb_3, InSb, and Zn is proposed. According to its DSC heating trace $Zn_5Sb_4In_{2-\delta}$ appears thermodynamically stable, which is in contrast with related materials, e.g., Cd_4Sb_3 and $Zn_9Sb_6In_2$,[12,22] where broad exothermic events upon heating reveal a metastable nature.

Several ex-situ investigations were also performed. For this selected crystals and polycrystalline powder, samples of $Zn_5Sb_4In_{2-\delta}$ were sealed under vacuum in silica ampoules, annealed for three hours at different temperatures, and subsequently quenched. PXRD patterns of samples annealed at 673 K showed small amounts of Zn and InSb which drastically increased at 723 and especially 773 K (Fig. 6). The results from the ex-situ experiments indicate a thermal instability of $Zn_5Sb_4In_{2-\delta}$ which was not apparent from the DSC experiments. This was confirmed from long time (24 h) annealing experiments of disks obtained from specimen B. SEM revealed that $Zn_5Sb_4In_{2-\delta}$ actually slowly decomposes already at temperatures as low as 473 K. The decomposition manifests itself in the appearance of islands of segregated Zn on the surface, as shown in Fig. 7. We, therefore, conclude that, in contrast with earlier assumptions,[9,12] $Zn_5Sb_4In_{2-\delta}$ is metastable with respect to a decomposition into Zn, InSb, and Zn_4Sb_3 and only slow kinetics prevents the observation of an associated exothermic event in DSC.

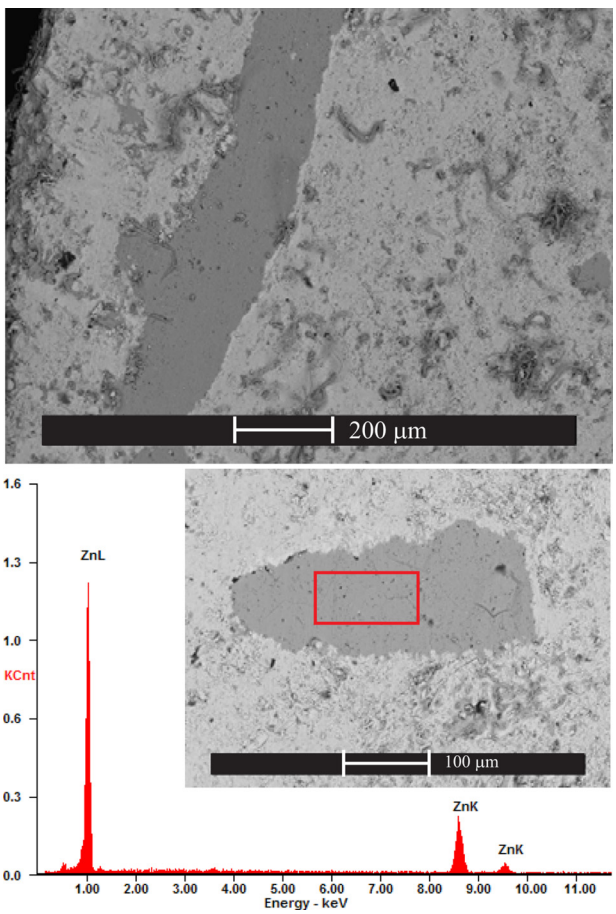

FIG. 7. Backscattering SEM images for a sample $Zn_5Sb_4In_{2-\delta}$ annealed at 473 K for 24 h showing islands and threads of segregated Zn.

IV. CONCLUSION

$Zn_5Sb_4In_{2-\delta}$ shows promising thermoelectric properties below room temperature. The values and temperature dependence of the electrical resistivity and thermopower are consistent with a doped narrow-gap semiconductor. At first sight, $Zn_5Sb_4In_{2-\delta}$ has many similarities to the state-of-the-art thermoelectrics Zn_4Sb_3; both materials display an order-disorder structural transition below room temperature, p-type conductivity, and non-stoichiometry. For Zn_4Sb_3, non-stoichiometry refers to the Zn composition which is additionally slightly variable. The Zn content of Zn_4Sb_3 defines the carrier concentration. This may be similar for $Zn_5Sb_4In_{2-\delta}$ with respect to its In composition, however, a detailed investigation into the phase width and its possible relation to charge carrier concentration has not been performed yet. The order-disorder transition in $Zn_5Sb_4In_{2-\delta}$ occurs at around 180 K and a process of carrier activation at around 220 K. The events do not appear connected. Carrier activation leads to a discontinuous change in the thermopower and electrical resistivity and as a consequence thermoelectric properties of $Zn_5Sb_4In_{2-\delta}$ degrade. Additionally, the material appears metastable and decomposes into Zn, InSb, and Zn_4Sb_3 at higher temperatures (above 450 K). Therefore, it seems unlikely that $Zn_5Sb_4In_{2-\delta}$ can be developed into a practical thermoelectric material.

ACKNOWLEDGMENTS

This work was supported by the National Science Foundation through grant DMR-1007557.

[1]G. J. Snyder and E. S. Toberer, Nature Mater. **7**, 105 (2008).
[2]S. G. Kim, I. I. Mazin, and D. J. Singh, Phys. Rev. B **57**, 6199 (1998).
[3]C. S. Birkel, E. Mugnaioli, T. Gorelik, U. Kolb, M. Panthöfer, and W. Tremel, J. Am. Chem. Soc. **132**, 9881 (2010).
[4]P. H. M. Böttger, G. S. Pomrehn, G. J. Snyder, and T. G. Finstad, Phys. Status Solidi A **208**, 2753 (2011).
[5]T. Caillat, J.-P. Fleurial, and A. Borshchevsky, J. Phys. Chem. Solids **58**, 1119 (1997).
[6]G. J. Snyder, M. Christensen, E. Nishibori, T. Caillat, and B. B. Iversen, Nature Mater. **3**, 458 (2004).
[7]B. B. Iversen, J. Mater. Chem. **20**, 10778 (2010).
[8]G. S. Pomrehn, E. S. Toberer, G. J. Snyder, and A. van de Walle, Phys. Rev. B **83**, 094106 (2011).
[9]Y. Wu, S. Lidin, T. L. Groy, N. Newman, and U. Häussermann, Inorg. Chem. **48**, 5996 (2009).
[10]U. Häussermann and A. S. Mikhaylushkin, Dalton Trans. **39**, 1036 (2010).

Downloaded 30 Jul 2012 to 131.215.220.186. Redistribution subject to AIP license or copyright; see http://jap.aip.org/about/rights_and_permissions

[11]E. S. Toberer, P. Rauwel, S. Gariel, J. Taftoe, and G. J. Snyder, J. Mater. Chem. **20**, 9877 (2010).
[12]Y. Wu, A. Tengå, S. Lidin, and U. Häussermann, J. Solid State Chem. **183**, 1574 (2010).
[13]E. Stoyanov, U. Häussermann, and K. Leinenweber, High Press. Res. **30**, 175 (2010).
[14]L. J. van der Pauw, Philips Res. Repts. **13**, 1 (1958).
[15]H. Goldsmid and J. Sharp, J. Electr. Mater. **28**, 869 (1999).
[16]S. Bhattacharya, R. P. Hermann, V. Keppens, T. M. Tritt, and G. J. Snyder, Phys. Rev. B **74**, 134108 (2006).
[17]M. Fox, *Optical Properties of Solids* (Oxford University Press, 2010).
[18]A. P. Litvinchuk, B. Lorenz, F. Chen, J. Nylén, U. Häussermann, S. Lidin, L. Wang, and A. M. Guloy, Appl. Phys. Lett. **90**, 181920 (2007).
[19]E. S. Toberer, C. A. Cox, S. R. Brown, T. Ikeda, A. F. May, S. M. Kauzlarich, and G. J. Snyder, Adv. Funct. Mater. **18**, 2795 (2008).
[20]E. S. Toberer, A. Zevalkink, N. Crisosto, and G. J. Snyder, Adv. Funct. Mater. **20**, 4375 (2010).
[21]A. Zevalkink, E. S. Toberer, W. G. Zeier, E. Flage-Larsen, and G. J. Snyder, Energy Environ. Sci. **4**, 510 (2011).
[22]A. Tengå, S. Lidin, J.-P. Belieres, N. Newman, Y. Wu, and U. Häussermann, J. Am. Chem. Soc. **130**, 15564 (2008).

Downloaded 30 Jul 2012 to 131.215.220.186. Redistribution subject to AIP license or copyright; see http://jap.aip.org/about/rights_and_permissions